Winter sea-ice melt in the Canada Basin, Arctic Ocean

Jennifer M. Jackson,[1,2] William J. Williams,[3] and Eddy C. Carmack[3]

Received 2 November 2011; revised 18 January 2012; accepted 18 January 2012; published 15 February 2012.

[1] Recent warming and freshening of the Canada Basin has led to the year-round storage of solar radiation as the near-surface temperature maximum (NSTM). Using year-round ocean (from ice tethered profilers and autonomous ocean flux buoys), sea-ice (from ice mass balance buoys), and atmosphere (from NCEP/NCAR reanalysis) data from 2005–2010, we find that heat from the NSTM is entrained into the surface mixed layer (SML) during winter. Entrainment can only occur when the base of the SML reaches the top of the NSTM. If this condition is met, the surface forcing and stratification together determine whether the SML deepens into the NSTM. Heat transfer occurs by diffusion or by the erosion of the summer halocline. The average temperature of the SML warmed by as much as 0.06°C during storm events. Solar radiation began warming the SML about 1 month early during the winter of 2007–2008 and this can be explained by thin sea ice. **Citation:** Jackson, J. M., W. J. Williams, and E. C. Carmack (2012), Winter sea-ice melt in the Canada Basin, Arctic Ocean, *Geophys. Res. Lett.*, *39*, L03603, doi:10.1029/2011GL050219.

1. Introduction

[2] Since the early 1990s, warming [*Perovich et al.*, 2007] and freshening [e.g., *Steele et al.*, 2010] of the near surface waters of the Canada Basin, Arctic Ocean (Figure 1) have altered the water mass structure of the upper 100 m [*Jackson et al.*, 2010; *Toole et al.*, 2010; *Jackson et al.*, 2011]. The surface mixed layer (SML) has shoaled from an average depth of 40–50 m (based on data from the 1890s to 1970s) [*Coachman and Barnes*, 1961; *Morison and Smith*, 1981] to an average surface mixed layer depth (SMLD) of 16 m in summer and 24 m in winter [*Toole et al.*, 2010]. The base of the SML in summer is the summer halocline that is formed by sea ice melt diluting the SML [*Jackson et al.*, 2010]. The summer halocline separates the SML from the near-surface temperature maximum (NSTM), a feature that is formed each summer by heat from solar radiation that is trapped by the stratification of the summer halocline [*Jackson et al.*, 2010; *Steele et al.*, 2011].

[3] Data from 1993 to 2009 show the summer NSTM has warmed by up to 1.5°C in summer [*Jackson et al.*, 2011] and has been observed throughout winter [*Jackson et al.*, 2010; *Steele et al.*, 2011]. Can heat from the NSTM melt ice during winter? *Toole et al.* [2010] suggest that the strengthening summer halocline (due to increased sea ice melt and subsequent freshening of the SML) prevents heat from the NSTM from escaping into the SML. However, using a 1-D model, *Jackson et al.* [2011] found that over one year, diffusion from the NSTM can warm the SML by up to 0.2°C. It is also possible that storms that deepen the SML can erode the summer halocline since *Yang et al.* [2004] found that winter storms with wind speeds greater than 10 ms^{-1} could deepen the SML to at least 45 m. Here we examine year-round CTD data from Ice Tethered Profilers (ITP), sea ice thickness data from an ice mass balance (IMB) buoy, ocean flux data from an autonomous ocean flux buoy (AOFB), and NCEP/NCAR reanalysis data to demonstrate that heat is released from the NSTM to the SML during winter and that heat can melt sea ice. Examples are highlighted to show that mixing events that entrain heat from the NSTM require SML depths to reach the top of the NSTM and erode the stratification there.

2. Data and Methods

[4] To examine the upper ocean properties, we use year-round archived (level 3) CTD data from Ice Tethered Profilers (ITP) [*Toole et al.*, 2006; *Krishfield et al.*, 2008] (http://www.whoi.edu/itp). We use 3 instruments: instrument number 1 (ITP1), which sampled under a 4.6 m ice floe from 16 August, 2005–31 August, 2006; instrument number 18 (ITP18), which sampled under a 3.1 m ice floe from 16 August, 2007–31 July, 2008; and instrument number 33 (ITP33), which sampled under a 4.2 m ice floe from 7 October, 2009–31 August, 2010. These ITPs are chosen because they collect data in roughly the same region for the same length of time and together span a period of rapid sea ice melt and NSTM warming. We do not consider all available ITP data here, as our focus is to demonstrate the effect of heat transfer from the NSTM to the SML rather than to develop parameterizations. Uncertainties in the CTD data are estimated at 0.005 psu practical salinity units and 0.005°C [*Krishfield et al.*, 2008]. Data collection commences at about 8 m and continues to 800 m with 1 m resolution. Daily profiles are examined and those that started deeper than 10 m are ignored.

[5] Following the new thermodynamic equation of seawater [*IOC et al.*, 2010], conservative temperature (°C) and absolute salinity (g kg^{-1}) are calculated from in-situ temperature and practical salinity collected by each ITP. Absolute salinity and conservative temperature are then used to calculate density (kg m^{-3}), freezing temperature (°C), and the buoyancy frequency (s^{-1}). To assess the impact of SML temperature on the sea ice, potential temperature and freezing temperature are calculated relative to the pressure at the base of sea ice, estimated from the thickness of the ice floe.

[1]Department of Oceanography, University of Cape Town, Cape Town, South Africa.
[2]Now at Applied Physics Laboratory, University of Washington, Seattle, Washington, USA.
[3]Institute of Ocean Sciences, Fisheries and Oceans Canada, Sidney, British Columbia, Canada.

0094-8276/12/2011GL050219

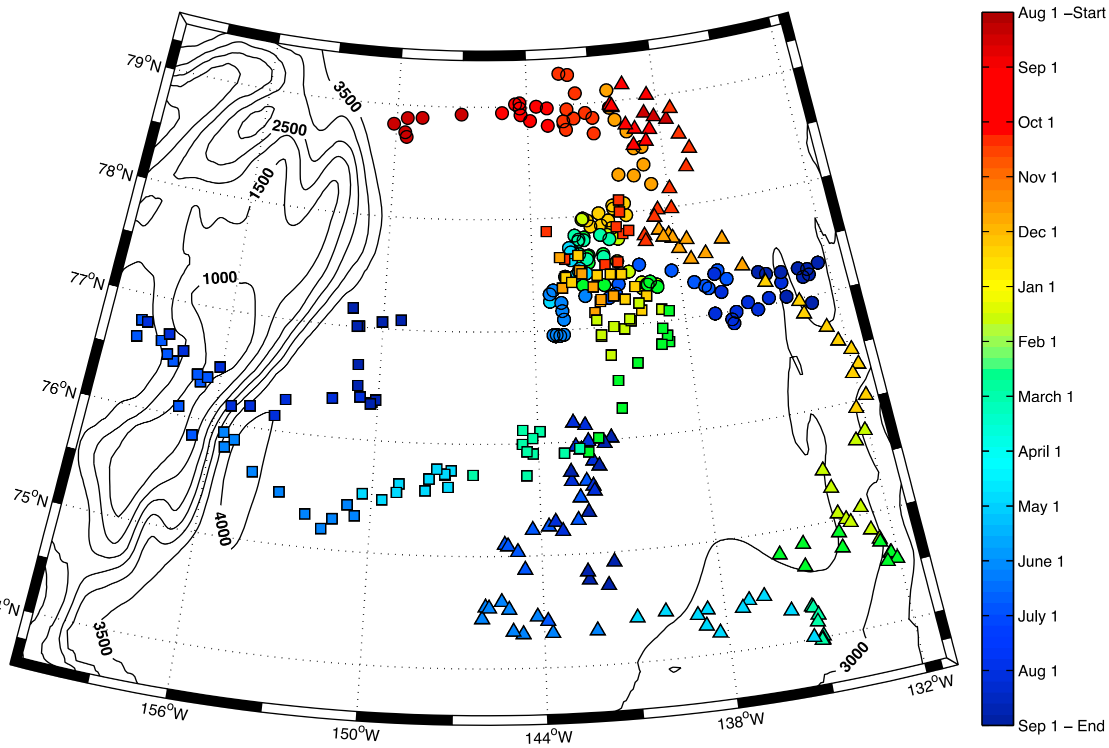

Figure 1. Locations of each ITP within the Canada Basin. The black contour lines show the bathymetry in 500 m intervals from 500 m to 4000 m. Each ITP has a different symbol that is coloured by time of year: ITP1 (circles) collected data from 16 August, 2005–31 August, 2006, ITP18 (triangles) collected data from 16 August, 2007–31 August, 2008, and ITP33 (squares) collected data from 7 October, 2009–31 August, 2010.

[6] During the winter's dark periods, virtually no solar radiation is available to heat the Arctic Ocean. Thus, during winter, if the observed temperature of the SML (T) increases above the freezing temperature (T_f), or T-$T_f > 0$, it suggests heat loss from the NSTM. Heat transfer from the NSTM to the SML could occur either through diffusion or through the erosion of the summer halocline by wind or ice-motion driven mixing. To track the temperature of the SML, we first define the SMLD based on a density difference criterion. We use two different criteria - one defines the SMLD as the first depth where the density difference is greater than 0.01 $\mathrm{kgm^{-3}}$ relative to the density at 8 m (similar to the definition used by *Toole et al.* [2010]) and the other uses a greater density difference of 0.03 $\mathrm{kgm^{-3}}$. SMLD definitions have been debated [e.g., *Kara et al.*, 2000] and we use two different criteria to ensure that the definition did not alter our results. We then calculate the average T-T_f within the SML for both definitions of SMLD.

[7] An IMB (IMB 2007F [*Perovich et al.*, 2009]) and an AOFB buoy (AOFB13 [*Shaw et al.*, 2008]) were deployed beside ITP18 from the winter of 2007–2008. Following the method outlined by *Krishfield and Perovich* [2005], GPS (to estimate ice speed), ADCP (to measure ocean velocity), and CTD data (to evaluate the absolute temperature below the ice) from the AOFB buoy are used to estimate the ocean heat flux. No IMB or AOFB were deployed with ITP1 or ITP33.

[8] We estimate wind speed using the daily averaged u and v wind speed at 10 m from NCEP/NCAR reanalysis data [*Kalnay et al.*, 1996] to calculate the total wind speed at 10 m ($U_{10} = \sqrt{(u^2 + v^2)}$). ITPs move with the ice, thus we could not use wind data from the same location throughout the year. To account for the movement of each ITP, we average its location every 2 weeks and use data from the nearest NCEP/NCAR coordinate.

3. Results

3.1. ITP1, 2005–2006

[9] Results from ITP1 show the presence of an NSTM that is about 0.3°C above the freezing temperature at a depth of 10–25 m from at least mid-August through the beginning of October (Figure 2a). The SML deepens at the beginning of September (Figures 2a and 2b) and a T-$T_f > 0$ is observed until the beginning of November (Figure 2c). During this time, the SMLD is located just above the NSTM (Figure 2d).

[10] The strongest winds (with a maximum daily average of over 14 $\mathrm{ms^{-1}}$), and fastest ITP (ice) speeds (with a maximum daily average of over 0.2 $\mathrm{ms^{-1}}$) are observed at the end of October (see event 1 in Figure 2). At this same time, the SML deepens by about 10 m and the absolute temperature of the SML increases by 0.04°C. Both wind speed (R^2 = 0.89, p-value = 0.02, see auxiliary material) and ITP speed (R^2 = 0.99, p-value = 0.00 - not shown) are well-correlated with the temperature of the SML one day later for the 5 days surrounding the storm.[1] Relative to ITP18 and ITP33, stratification is weaker throughout this winter and also less variable (Figures 2f and S1). The combination of weaker stratification and SML depths close to the top of the NSTM

[1]Auxiliary materials are available in the HTML. doi:10.1029/2011GL050219.

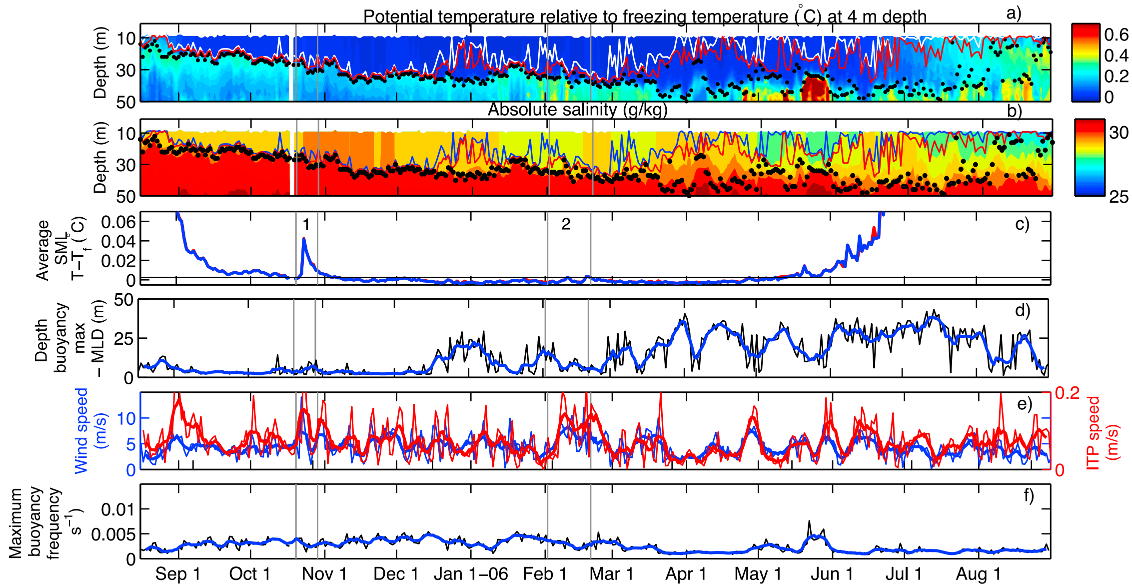

Figure 2. Results from ITP1. (a) The observed temperature relative to the freezing temperature (T-T_f) at the base of the ice floe (4 db) as colour contours. The SMLD is shown that is defined by both the smaller (white line; 0.01 kgm^{-3}) and larger (red line; 0.03 kgm^{-3}) density differences. The depth of the maximum buoyancy frequency is shown as black dots. (b) Similar to Figure 2a, coloured contours are absolute salinity, however the blue line indicates the SMLD calculated with the smaller density difference. (c) The average T-T_f of the SML using both the smaller (blue line) and larger (red line) density difference. The black horizontal line shows the temperature error range from the CTD. (d) Depth difference between the buoyancy frequency maximum (synonymous with the top of the NSTM) and the SMLD, (e) daily averaged wind speed from the NCEP/NCAR reanalysis (blue lines) and the daily averaged ITP speed (red lines), and (f) the value of the maximum buoyancy frequency. In Figures 2d–2f, the thin line is the daily value and the thick line is the 5 day centred running mean. The pairs of vertical grey lines bracket events discussed in the text, which are numbered in Figure 2c).

during event 1 sets the stage for strong wind and fast ice motion to cause deepening of the mixed layer that entrains heat from the NSTM.

[11] The SMLD and NSTM are about the same depth until mid-December, when the SMLD shoals while the NSTM continued to deepen (Figure 2a). The SML freshens at the beginning of December, possibly because ITP1 drifted into the edge of the Beaufort Gyre [*Jackson et al.*, 2011], while the salinity of the NSTM remains constant and this salinity difference can explain the different depths of the NSTM and SML. This depth difference influences the amount of heat lost from the NSTM. For example, a series of strong storms occurs at the beginning of February and the SML deepens by about 10 m. During this time the SML warms only slightly since the top of the NSTM (~35–45 m) remains about 5–10 m deeper than the SMLD (~25–35 m) (Figure 2d). There are several occurrences where the NSTM appears to shoal and two of these events (17 January and 18 February, 2006) are caused by the passage of a shallow eddy [*Timmermans et al.*, 2008]. This suggests that shallow eddies could enhance heat loss from the NSTM if present at the same time as a storm. Solar radiation warms the SML in mid-May and the SML shoals at the end of June.

3.2. ITP18, 2007–2008

[12] Results from ITP18 show that the temperature of the NSTM is as high as 0.7°C above freezing in the summer of 2007 (Figure 3a). Similar to ITP1, the SML cools and deepens in mid-September (Figure 3b) and the SML temperature returns to near-freezing by mid-October. A moderate storm, with a maximum daily wind speed of 10 ms^{-1} but with a relatively low ITP speed of ~0.1 ms^{-1}, occurs in mid-November (event 1 in Figure 3) and the SML deepens by more than 10 m bringing the base of the SML close to the maximum stratification at the top of the NSTM (Figure 3d). After this initial deepening, strong stratification appears to prevent further SML deepening and the entrainment of NSTM heat into the SML (Figure 3c). During the month of December, winds are weak yet there is a spike in SML temperature which reaches almost 0.05°C above freezing (event 2 in Figure 3). During this time, ITP18 drifts east into a region with a very shallow NSTM (10 m) and it is likely that the short vertical distance between the NSTM and SMLD (Figure 3d) and weak stratification (Figure 3f) allows heat to diffuse from the NSTM to the SML. Another spike in SML temperature occurs in mid February 2008 (event 3 in Figure 3) with temperatures rising to almost 0.06°C above freezing, and this appears to be due to a weak winter storm (but with moderate ITP speeds of over 0.2 ms^{-1}) that causes the entrainment of a relatively shallow NSTM. The SML warms at the beginning of April, about 1 month earlier than 2006. The NSTM is much deeper than the SML for most of April (Figures 3a and 3d) and this suggests it is solar radiation and not the NSTM that warms the SML.

3.3. ITP33, 2009–2010

[13] Data collection from ITP33 begins in the fall of 2009, after the SML had deepened (Figure 4). The NSTM below the SML is very warm, up to 0.8°C above freezing. Throughout winter, the average SML temperature is often

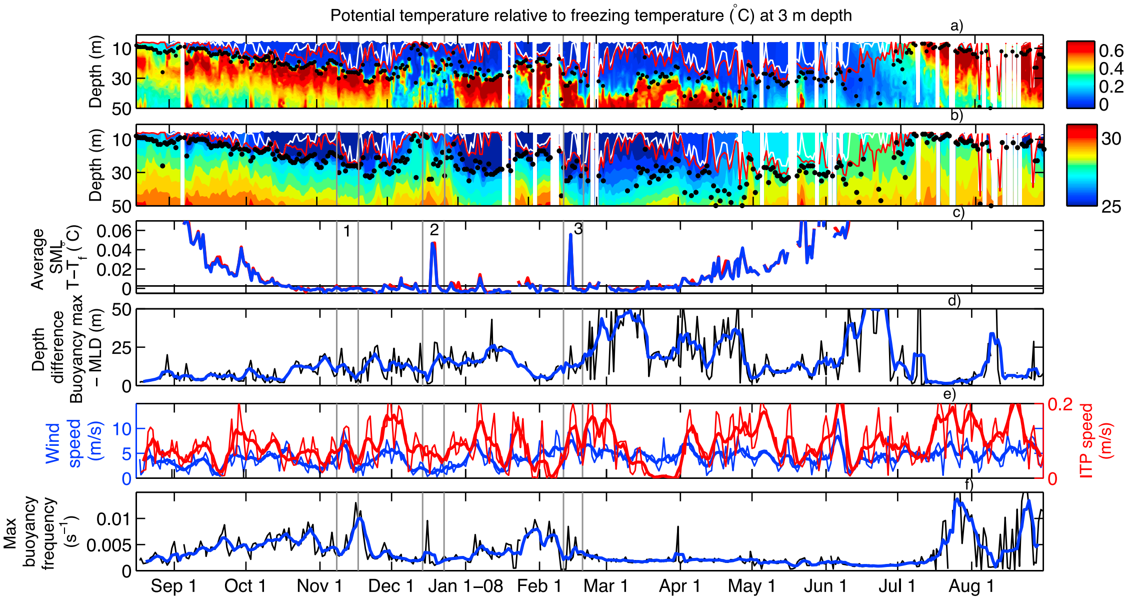

Figure 3. As for Figure 2 but for ITP18.

marginally above the freezing temperature (Figure 4c) and neither high wind speed nor weak stratification can explain the warm SML (see auxiliary material). However, the SML is usually just above the NSTM (Figures 4a and 4d) and the ice speed is consistently high (Figure 4e). For example, warming events 1 and 2 occur when the maximum buoyancy frequency is the same depth as the SMLD and the ice speed is greater than 0.15 ms^{-1}. These results suggest that, unlike a strong winter storm in the winter of 2005–06 and a shallow NSTM in the winter of 2007–2008, the winter 2009–2010 warm events are primarily caused by fast ice and a warm NSTM temperature. In addition, the small vertical distance between the NSTM and the SMLD likely enhances temperature diffusion, providing some continual warming of the SML. The buoyancy frequencies are relatively high until April (Figure 4f) and this stratification likely minimizes heat loss from the NSTM due to storms. The SML warms at the beginning of May, about 1 month later than was observed in 2008.

4. Discussion

[14] Observations from ITP1, ITP18, and ITP33 suggest several mechanisms that enable the erosion of the summer halocline and the release of heat from the NSTM into the SML. These mechanisms are high wind speeds (a daily average of about 10 ms^{-1}), high ice speeds (a daily average of about 0.15 ms^{-1}), a SMLD that reaches the top of the NSTM, and weak stratification (a maximum buoyancy frequency of less than 0.006 s^{-1}).

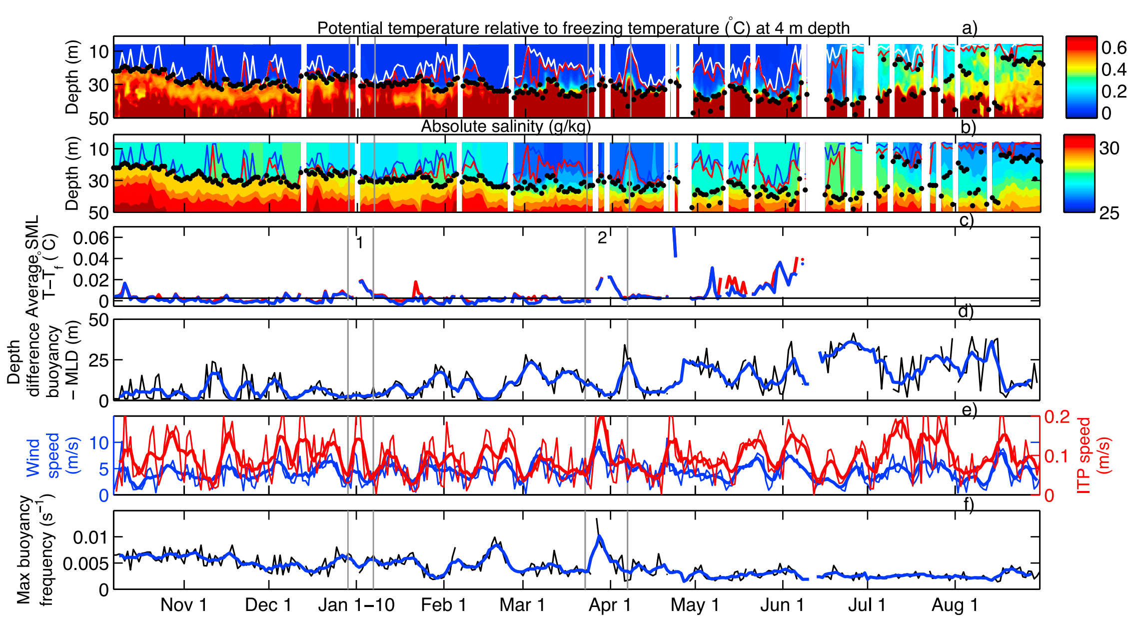

Figure 4. As for Figure 2 but for ITP33.

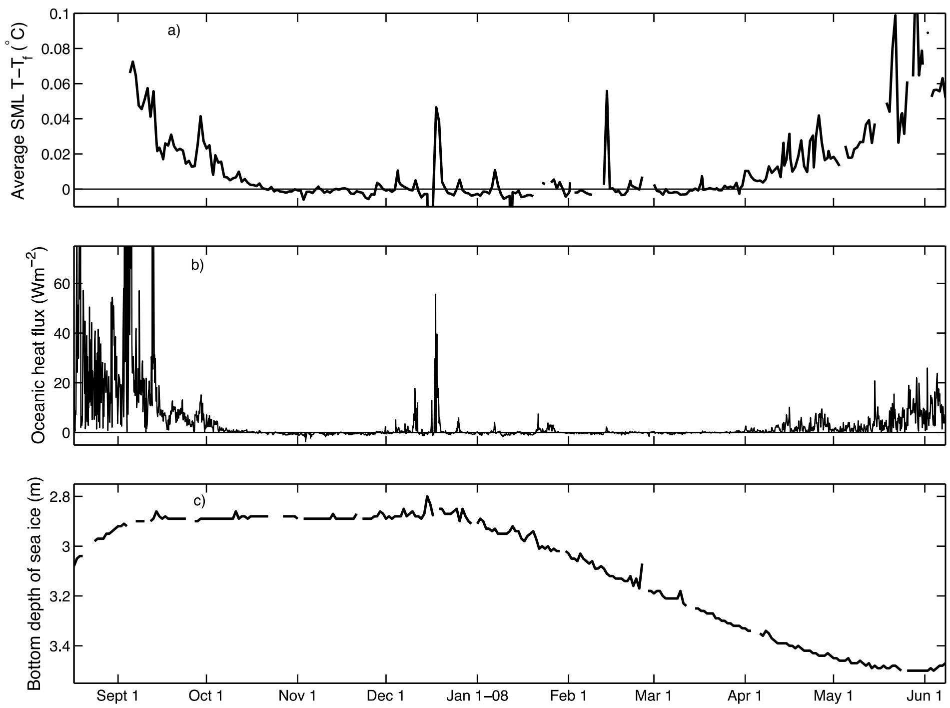

Figure 5. A comparison between (a) the SML T-T$_f$ for ITP18 (°C), (b) the oceanic heat flux (Wm^{-2}) calculated from the autonomous ocean flux buoy, and (c) the bottom depth of sea ice (m) measured from the ice mass balance buoy. Data are from 16 August 2007–6 June, 2008.

[15] The processes that transfer heat from the NSTM to the SML are:

1. The continual diffusion of heat from the NSTM to the SML. As shown by *Jackson et al.* [2011], heat diffuses from the NSTM to the SML through winter. A strong temperature gradient across a pycnocline increases diffusive flux [*Martinson*, 1990], thus diffusion is strongest when there is a large temperature gradient between the NSTM and SML. As is observed during the winter of 2009–2010, the impact of diffusion is enhanced by a short vertical distance between the SMLD and the NSTM.

2. The gradual weakening of the summer halocline throughout winter. This weakening is likely caused by the cumulative effect of wind and ice mixing and brine rejection. Data from ITP1, ITP18, and ITP33 suggest that the summer halocline is weakest in spring, sometime between March and May.

3. The rapid erosion of the summer halocline by episodic events. Our results suggest that winter storms with wind speeds of at least 10 ms^{-1} can cause abrupt erosion of the summer halocline. Storms are most effective at eroding the summer halocline when the NSTM and SML are shallow or when stratification is weak. Ekman pumping from the anticyclonic (convergent) Beaufort Gyre causes the NSTM to deepen [*Jackson et al.*, 2010], with greatest downwelling rates in fall [*Yang*, 2006] thus we suggest that storms are most effective at eroding the NSTM in early fall, before the NSTM deepens.

5. Impact on the Winter Sea Ice Cover

[16] Results from an IMB buoy and an AOFB buoy deployed beside ITP18 suggest that heat from the NSTM melts winter sea ice (Figure 5). Several of the warming events identified in section 3.2 are evident in the ocean heat flux data. In particular, a heat flux of up to 55 Wm^{-2} is observed when ITP18 drifts into a region with a shallow NSTM in early to mid-December. IMB data suggest sea ice melt during this event. Another period of rapid ice melt is observed in late February that is associated with a SML that is above the freezing temperature. IMB data also show that the ice floe is thinnest (2.8 m) in mid-December - about 2 months later than observed during the winter of 1997–1998 [*Perovich et al.*, 2003]. The SML warms in April 2008 and since sea ice is about 1 m thinner in 2008 than 2006 or 2010, we suggest that the delayed growth and melting of sea ice through the winter of 2007–2008 allows solar radiation to enter the SML one month early. These results suggest that the release of heat from the NSTM to the SML both delays the growth of sea ice and episodically melts sea ice during winter.

[17] **Acknowledgments.** We acknowledge financial support from Fisheries and Oceans Canada and the National Research Foundation of South Africa. The Ice-Tethered Profiler data were collected and made available by the Ice-Tethered Profiler Program based at the Woods Hole Oceanographic Institution (http://www.whoi.edu/itp). The ice-mass balance buoy data are made available by the Cold Regions Research and Engineering Laboratory (http://imb.crrel.usace.army.mil/massbal.htm). The autonomous ocean flux buoy data are provided by the Naval Postgraduate School (http://www.oc.nps.edu/). The NCEP Reanalysis data were provided by the NOAA/OAR/ESRL PSD, Boulder, Colorado, USA, from their Web site at http://www.esrl.noaa.gov/psd/.

[18] The Editor thanks two anonymous reviewers for their assistance in evaluating this paper.

References

Coachman, L. K., and C. A. Barnes (1961), The contribution of Bering Sea water to the Arctic Ocean, *Arctic*, *14*, 146–161.

IOC, SCOR, and IAPSO (2010), *The International Thermodynamic Equation of Seawater—2010: Calculation and Use of Thermodynamic Properties, Manuals Guides*, vol. 56, 196 pp., UNESCO, Paris.

Jackson, J. M., E. C. Carmack, F. A. McLaughlin, S. E. Allen, and R. G. Ingram (2010), Identification, characterization, and change of the near-surface temperature maximum in the Canada Basin, 1993–2008, *J. Geophys. Res.*, *115*, C05021, doi:10.1029/2009JC005265.

Jackson, J. M., S. E. Allen, F. A. McLaughlin, R. A. Woodgate, and E. C. Carmack (2011), Changes to the near-surface waters in the Canada Basin, Arctic Ocean from 1993–2009: A basin in transition, *J. Geophys. Res.*, *116*, C10008, doi:10.1029/2011JC007069.

Kalnay, E., et al. (1996), The NCEP/NCAR 40-year reanalysis project, *Bull. Am. Meteorol. Soc.*, *77*(3), 437–471.

Kara, A. B., P. A. Rochford, and H. E. Hurlburt (2000), An optimal definition for ocean mixed layer depth, *J. Geophys. Res.*, *105*(C7), 16,803–16,821.

Krishfield, R. A., and D. K. Perovich (2005), Spatial and temporal variability of oceanic heat flux to the Arctic ice pack, *J. Geophys. Res.*, *110*, C07021, doi:10.1029/2004JC002293.

Krishfield, R., J. Toole, A. Proshutinsky, and M.-L. Timmermans (2008), Automated ice-tethered profilers for seawater observations under pack ice in all seasons, *J. Atmos. Oceanic Technol.*, *25*(11), 2091–2105.

Martinson, D. G. (1990), Evolution of the Southern Ocean winter mixed layer and sea ice: Open ocean deepwater formation and ventilation, *J. Geophys. Res.*, *95*(C7), 11,641–11,654.

Morison, J., and J. D. Smith (1981), Seasonal variations in the upper Arctic Ocean as observed at T-3, *Geophys. Res. Lett.*, *8*(7), 753–756.

Perovich, D. K., T. C. Grenfell, J. A. Richter-Menge, B. Light, W. B. Tucker III, and H. Eicken (2003), Thin and thinner: Sea ice mass balance measurements during SHEBA, *J. Geophys. Res.*, *108*(C3), 8050, doi:10.1029/2001JC001079.

Perovich, D. K., B. Light, H. Eicken, K. F. Jones, K. Runciman, and S. V. Nghiem (2007), Increasing solar heating of the Arctic Ocean and adjacent seas, 1979–2005: Attribution and role in the ice-albedo feedback, *Geophys. Res. Lett.*, *34*, L19505, doi:10.1029/2007GL031480.

Perovich, D. K., J. A. Richter-Menge, B. Elder, K. Claffey, and C. Polashenski (2009), Observing and understanding climate change: Monitoring the mass balance, motion, and thickness of Arctic sea ice, report, Cold Reg. Res. and Eng. Lab., Hanover, N. H. [Available at http://IMB.crrel.usace.army.mil.]

Shaw, W. J., T. P. Stanton, M. G. McPhee, and T. Kikuchi (2008), Estimates of surface roughness length in heterogeneous under-ice boundary layers, *J. Geophys. Res.*, *113*, C08030, doi:10.1029/2007JC004550.

Steele, M., J. Zhang, and W. Ermold (2010), Mechanisms of summertime upper Arctic Ocean warming and the effect on sea ice melt, *J. Geophys. Res.*, *115*, C11004, doi:10.1029/2009JC005849.

Steele, M., W. Ermold, and J. Zhang (2011), Modeling the formation and fate of the near-surface temperature maximum in the Canadian Basin of the Arctic Ocean, *J. Geophys. Res.*, *116*, C11015, doi:10.1029/2010JC006803.

Timmermans, M.-L., J. Toole, A. Proshutinsky, R. Krishfield, and A. Plueddemann (2008), Eddies in the Canada Basin, Arctic Ocean, observed from ice-tethered profilers, *J. Phys. Oceanogr.*, *38*(1), 133–145.

Toole, J., et al. (2006), Ice-tethered profilers sample the upper Arctic Ocean, *Eos Trans. AGU*, *87*(41), 434, doi:10.1029/2006EO410003.

Toole, J. M., M.-L. Timmermans, D. K. Perovich, R. A. Krishfield, A. Proshutinsky, and J. A. Richter-Menge (2010), Influences of the ocean surface mixed layer and thermohaline stratification on Arctic Sea ice in the central Canada Basin, *J. Geophys. Res.*, *115*, C10018, doi:10.1029/2009JC005660.

Yang, J., J. Comiso, D. Walsh, R. Krishfield, and S. Honjo (2004), Storm-driven mixing and potential impact on the Arctic Ocean, *J. Geophys. Res.*, *109*, C04008, doi:10.1029/2001JC001248.

Yang, J. (2006), The seasonal variability of the Arctic Ocean Ekman transport and its role in the mixed layer heat and salt fluxes, *J. Clim.*, *19*, 5366–5387.

J. M. Jackson, Applied Physics Laboratory, University of Washington, 1013 NE 40th St., Seattle, WA 98105-6698, USA. (jjackson@apl.washington.edu)

E. C. Carmack and W. J. Williams, Institute of Ocean Sciences, Fisheries and Oceans Canada, PO Box 6000, Sidney, BC V8L 4B2, Canada. (eddy.carmack@dfo-mpo.gc.ca; bill.williams@dfo-mpo.gc.ca)